Journal of Mechatronics, Electrical Power, and Vehicular Technology 17 (2026) 180-193

Journal of Mechatronics, Electrical Power, and Vehicular Technology

e-ISSN: 2088-6985
p-ISSN: 2087-3379

mev.brin.go.id

Analytical optimization of displacer trajectory for ideal beta-type Stirling engine cycles with sinusoidal piston motion

Rachman Hakim [a, b], Toto Hardianto [c, *], Priyono Sutikno [d, e], Poetro Sambegoro [c]

[a] *Doctoral Program of Mechanical & Aerospace Engineering, Faculty of Mechanical & Aerospace Engineering, Institut Teknologi Bandung Jl. Ganesha No. 10, Bandung, 40132, Indonesia*

[b] *Faculty of Manufacturing Technology, Universitas Jenderal Achmad Yani Jl. Terusan Jenderal Sudirman, Cimahi, 40531, Indonesia*

[c] *Faculty of Mechanical and Aerospace Engineering, Institut Teknologi Bandung Jl. Ganesha No. 10, Bandung, 40132, Indonesia*

[d] *Department of Mechanical Engineering, Faculty of Engineering, Universitas Pasundan Jl. Dr. Setiabudi No. 193, Bandung, 40153, Indonesia*

[e] *Research Center on New and Renewable Energy, Institute for Research and Community Services (LPPM), Institut Teknologi Bandung Jl. Ganesha No. 10, Bandung, 40132, Indonesia*

Abstract

This study develops a generalized displacer motion equation for a beta-type Stirling engine. The proposed equation approximates the ideal Stirling cycle while maintaining sinusoidal piston motion to ensure stable power extraction. The displacer trajectory is modeled with a Fourier series and optimized. The resulting trajectory is then generalized as a piecewise function to improve applicability across different geometries. This approach improves control of working fluid distribution, allowing the expansion and compression processes to more closely approach isothermal conditions. The results show that the optimized Fourier trajectory achieves 91.9 % of the ideal Stirling-cycle work output, outperforming conventional drive mechanisms, where it only achieves 59.8 % for crank mechanism, 66 % for Scotch yoke, and 68.5 % for rhombic drive. For practical implementation, the optimized Fourier trajectory is generalized using a piecewise formulation. The generalized trajectory maintains approximately 80–90 % of the ideal Stirling-cycle work over a range of compression ratios without requiring re-optimization. These results demonstrate that the proposed approach provides both high thermodynamic performance and improved adaptability compared with conventional Stirling engine drive mechanisms.

Keywords: displacer control; displacer trajectory; Fourier trajectory; piecewise function; Stirling engine.

I. Introduction

The growing awareness of environmental problems and the limited global energy supply have led to the urgent need to develop sustainable energy generation systems [1]. Among promising energy generation systems, the Stirling engine has attracted considerable attention for its ability to utilize various renewable thermal energy sources, such as biomass and solar energy [2][3]. The abundant, near carbon-neutral thermal energy provided by biomass and sustainability, widespread availability, and high energy potential of solar energy further enhances the suitability of Stirling engines for renewable energy applications [4][5]. In

* Corresponding Author. totohardianto@itb.ac.id (T. Hardianto)

https://doi.org/10.55981/j.mev.2026.1486

Received 30 May 2026; revised 7 July 2026; accepted 13 July 2026; available online 30 July 2026; published 31 July 2026

How to Cite: R. Hakim *et al.*, "Analytical optimization of displacer trajectory for ideal beta-type stirling engine cycles with sinusoidal piston motion," *Journal of Mechatronics, Electrical Power, and Vehicular Technology*, vol. 17, no. 1, pp. 180-193, July, 2026.

addition, the Stirling engine offers significant operational flexibility, as it can operate effectively over a wide temperature range [6]. Theoretically, the maximum thermal efficiency of an ideal Stirling engine can reach Carnot thermal efficiency, which is based on a thermodynamic cycle involving two ideal isothermal processes and two ideal isochoric processes [7]. However, achieving operating conditions close to this ideal cycle is not easy because any deviation from the ideal thermodynamic processes reduces the thermal efficiency and power output of practical Stirling engines. Therefore, various strategies have been proposed to approach the ideal cycle, including improvements in heat transfer and volume dynamics [8][9].

The dynamic working-space volumes of a Stirling engine, including the hot-space, cold-space, and total volumes, are determined by the piston and displacer motions. The geometric arrangement of the piston and displacer within the cylinder is commonly used to classify Stirling engines into alpha, beta, and gamma-types [10]. The beta-type Stirling engine offers advantages for implementing controlled mechanisms. In beta-types, piston and displacer are in the same cylinder, allowing their motion to overlap [11]. This overlap provides thermodynamic and mechanical benefits compared to other types by reducing dead volume and facilitating a higher compression ratio (CR) [12]. Furthermore, the displacer and the power piston serve distinct functions. The displacer motion determines the variation of hot and cold volume, while the piston determines the variation of cold and total volume [13]. The displacer must properly control the distribution of the working fluid volume to approach the four ideal thermodynamic processes.

Conventional beta Stirling engines commonly use kinematic mechanisms, including crank, rhombic, and Scotch yoke [14]. However, the mechanism naturally limits the movement of the piston and displacer, resulting in primarily sinusoidal motion that deviates from the ideal motion [15][16]. The sinusoidal motion causes a portion of the working fluid to remain in other spaces during compression and expansion, preventing an isothermal process [17]. The actual thermal efficiency is only 66 % of the ideal value, which is 27.1 % lower than Carnot [18]. Inadequate synchronization of piston and displacer motion reduces heat-transfer efficiency, increases dead volume, decreases the CR, and reduces the engine's mechanical work [19]. The CR significantly influences the net work output, heat input, and efficiency of the Stirling engine. A lower CR results in reduced net work and efficiency, while the heat input increases.

Recent studies have explored the use of motion control and complex kinematic mechanisms to achieve motion characteristics that approximate those of the ideal Stirling cycle. Adaptive motion control strategies achieve optimal conditions by controlling the displacer position. Optimal Periodic Control (OPC) has been reported to increase power by up to 40 % compared to conventional kinematic systems [20]. Controlling both piston trajectories of the alpha-type via a variable-length connecting rod enables piston motion during a nearly constant-volume phase, resulting in a P–V trajectory that more closely approximates the ideal Stirling cycle than traditional alpha-type fixed-rod systems [21]. In addition to adaptive motion control at beta-type, mechanical innovations such as hypocycloid mechanisms allow the piston to remain at top dead center (TDC) and bottom dead center (BDC) longer than a traditional sinusoidal mechanism, thereby extending the duration of isochoric process [22]. A cam drive mechanism (CDM) on beta-type changes sinusoidal motion to make a dwell time phase at TDC and BDC. Tests show that this method can give 46 % more power than pure sinusoidal motion [23][24].

Although the existing approaches have improved performance through altering piston and displacer trajectories, their practical implementation remains limited. The main challenges lie in extracting power from the controlled piston and in the inherent complexity of the kinematic mechanism. In this study, a novel beta-type displacer trajectory was developed while maintaining sinusoidal piston motion. The developed motion equation enables the engine to achieve up to 90 % of the ideal cycle work. Moreover, the derived displacer motion equation is generally applicable to various engine geometries and CRs.

II. Materials and Methods

Controlled displacer and sinusoidal piston trajectories were implemented in a beta-type Stirling engine in this study, as shown in Figure 1. The beta-type configuration is selected due to the functional separation between the piston and the displacer. In this type, the piston handles compression and expansion, while the displacer pushes to distribute the working fluid [25]. The separation function enables control of the displacer without directly affecting the power generation process.

A. Formulation of piston motion under sinusoidal trajectory

The piston follows a sinusoidal motion, which ensures stable and efficient power extraction. This motion profile also facilitates easier coupling with

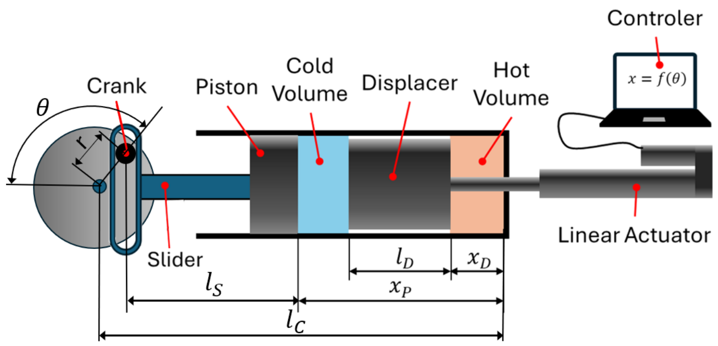

Figure 1. Schematic representation of a Stirling engine with a controlled displacer and a sinusoidal piston motion.

conventional generator systems, making it suitable for practical power-generation applications [11][24]. The piston sinusoidal motion profile is expressed by the following equation.

$$x_p(\theta) = l_c - r\cos(\theta + 135) - l_s \quad (1)$$

$$l_c = \frac{2r}{CR-1} + l_s + r \quad (2)$$

where x_p denotes piston position (m) as a function of the crank angle θ (deg), l_s is the stroke length (m), r is the crank radius (m), CR is the compression rasio, and l_c crank center to top of cylinder length (m).

$$CR = \frac{V_{max}}{V_{min}} \quad (3)$$

V_{max} and V_{min} denote the maximum and minimum fluid volumes within the cylinder (m^3), excluding the volumes of the regenerator, heater, and cooler. The sinusoidal motion of the piston maintains stable, efficient power extraction. It also makes it easy to couple with conventional generators.

B. Fourier series-based displacer motion modeling

Controlling the motion of the displacer requires less power than controlling the piston motion. Unlike the piston, the displacer does not compress the working fluid; it operates under a small pressure difference. A displacer requires only small power and can thus be actuated by a linear actuator. As a result, the displacer's motion can be flexibly adjusted and controlled independently.

The displacer position is modeled using a Fourier series to provide high flexibility in defining the optimal motion profile. The trajectory is expressed as a superposition of multiple harmonics, allowing precise adjustment through the Fourier coefficients. These parameters enable simultaneous control of amplitude and waveform characteristics. As a result, asymmetric trajectories can be generated to optimize the compression and expansion process. Moreover, using a Fourier series guarantees that the displacer trajectory remains continuous throughout a full cycle.

$$x_d(\theta) = s\,c_0 + \sum_{n=1}^{N} s\,a_n\cos(\theta) + s\,b_n\sin(\theta) \quad (4)$$

where x_d denotes displacer position (m), s represents the piston stroke (m), while c_0, a_n, and b_n denote the Fourier coefficients.

Fourier coefficients are used as the optimization variables to define the piston and displacer motion trajectories. The optimization objective is to maximize the net cyclic work, which corresponds to the area enclosed by the pressure–volume (p–V) diagram

$$W = \oint p\,dV \quad (5)$$

where W is the net work per cycle (J), p is the instantaneous working-gas pressure (Pa), and V is the instantaneous working volume (m^3). Numerical optimization is performed using the generalized reduced gradient (GRG) method [26].

The optimization is subject to the following constraints:

$$V_{min} \le V(t) \le V_{max} \quad (6)$$

which ensures that the working volume remains within the allowable geometric limits, and

$$\frac{mRT_C}{V(T)} \le p(t) \le \frac{mRT_H}{V(T)} \quad (7)$$

which constrains the pressure to remain between the limiting isothermal line corresponding to the cold and hot heat-source temperatures (see Figure 2). Here, $V_{\min}$ and $V_{\max}$ are the minimum and maximum working volumes (m^3), respectively, $p(t)$ is the instantaneous gas pressure (Pa), $V(t)$ is the instantaneous volume (m^3), m is the working-gas mass (kg), R is the specific gas constant (J/(kg·K)), and T_C and T_H denote the cold- and hot-space temperatures (K), respectively.

These constraints define the feasible thermodynamic search region by ensuring that the pressure trajectory remains between the limiting isothermal curves while satisfying the allowable working-volume range. These limiting curves represent the ideal Stirling-cycle boundary conditions, which consist of two isothermal processes and two constant-volume processes.

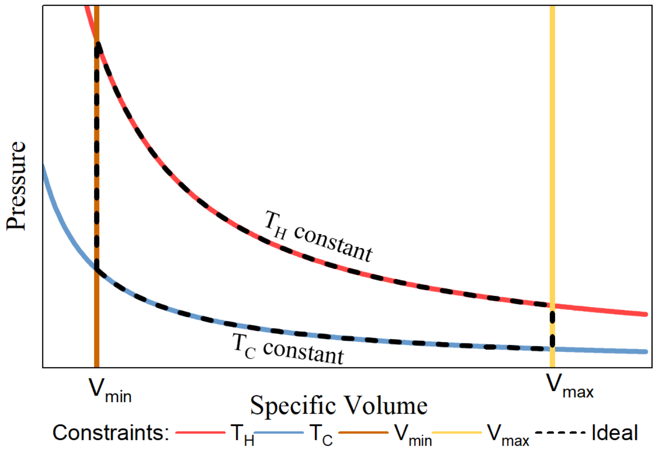

Figure 2. Optimization constraints in the p-V plane. The dashed line indicates the ideal Stirling-cycle boundary, while the colored lines represent the imposed isothermal and volume constraints.

Table 1.
Baseline engine parameters used in the optimization.

Parameter	Value
Working fluid	Air
Charge pressure (Pa)	101325
Hot reservoir temperature (K)	1000
Cold reservoir temperature (K)	300
Piston area (m^2)	0.002827
Piston stroke (m)	0.06

The GRG algorithm iteratively adjusts the Fourier coefficients to maximize the enclosed area of the p–V diagram under these ideal-cycle boundary conditions; therefore, the larger the enclosed area, the closer the cyclic work approaches the maximum work attainable by the ideal cycle. Consequently, the optimized trajectories are expected to yield cyclic work that approaches the ideal-cycle limit while satisfying all optimization constraints.

Baseline engine configuration was adopted throughout the trajectory optimization. Unless otherwise stated, all optimization results presented in this study were obtained using the same engine geometry and operating conditions. The baseline parameters are summarized in Table 1. Any modifications to the engine geometry required by specific drive mechanisms, such as variations in crank dimensions, are introduced and discussed separately in the corresponding comparison section.

C. Generalized displacer motion modeling using piecewise functions

In general, trajectory optimization applies to a specific geometric configuration, yielding solutions limited to those conditions. Consequently, the optimized trajectory cannot be directly applied to an engine with different geometrical parameters. Applying a Fourier-based trajectory to a different geometric configuration may reduce cycle performance. In certain cases, the mismatch of piston and displacer motion results in collisions between the piston and the displacer. Therefore, a generalized approach is required to overcome the limitations of the Fourier-based trajectory.

The displacer position is defined relative to the piston to ensure a generalized model. To facilitate the generalization process, the Fourier-based trajectory is divided into four segments corresponding to the ideal cycle process [27]. The ideal Stirling cycle consists of four thermodynamic processes: constant-volume heating (0° to 90°), isothermal expansion (90° to 180°), constant-volume cooling (180° to 270°), and isothermal compression (270° to 360°). During constant-volume heating, the cold volume decreases while the hot volume increases by an equal amount, maintaining a constant total working-gas volume as the gas is transferred from the cold side to the hot side. During isothermal expansion, the working gas occupies the hot volume, whereas the cold volume is minimized, allowing the total volume to increase at a constant hot-side temperature. During constant-volume cooling, the hot volume decreases while the cold volume increases by an equal amount, preserving a constant total working-gas volume as the gas is transferred back to the cold side. Finally, during isothermal compression, the working gas occupies the cold volume, whereas the hot volume is minimized, and the total volume decreases while the gas temperature remains constant at the cold-side temperature.

$$x_d(\theta) = \begin{cases} x_{d,0-90}(x_P), & 0^\circ \leq \theta \leq 90^\circ \\ x_{d,90-180}(x_P), & 90^\circ \leq \theta \leq 180^\circ \\ x_{d,180-270}(x_P), & 180^\circ \leq \theta \leq 270^\circ \\ x_{d,270-360}(x_P), & 270^\circ \leq \theta \leq 360^\circ \end{cases} \quad (8)$$

All segments were modeled using polynomial Lagrange interpolation. The formulation utilizes four reference points extracted from the optimized Fourier trajectory. The two boundary points that define the start (i=0) and end (i=3) of the segment, and two intermediate points that are evenly spaced between them (i=1 and i=2).

$$x_{d,segment} = \sum_{i=0}^{3} \sigma_i \, x_{p_i} \prod_{\substack{j=0 \\ j\neq i}}^{3} \frac{\theta-\theta_j}{\theta_i-\theta_j} \tag{9}$$

where σ represents the shape constant, it expresses the normalized Fourier-based displacer position relative to the piston position.

D. Thermodynamic model

The Schmidth method is widely used to represent the influence of piston and displacer kinematics on the Stirling cycle [28]. It simplifies heat transfer by assuming isothermal processes in the hot and cold spaces. The Schmidth formulation models the instantaneous pressure as a function of the volume distribution and the temperature of the hot volume and cold volume;

$$p = \frac{MR}{\left(\frac{V_C}{T_C}+\frac{V_H}{T_H}\right)} \tag{10}$$

where p is the instantaneous working-gas pressure (Pa), M is the total mass of the working gas (kg), V_H and V_C are the instantaneous hot and cold volumes (m^3), respectively, and T_H and T_C are the constant temperatures of the hot and cold spaces (K).

The instantaneous hot and cold volumes are determined from the displacer and piston positions as

$$V_H = x_d \, A_p \tag{11}$$

$$V_C = (x_P - x_d)\, A_P \tag{12}$$

where A_p is piston area (m^2).

The total mass of the working gas is assumed constant throughout the cycle and is calculated from the ideal gas equation using the initial engine state,

$$M = \frac{p_0 \; max(V_{H,o}+V_{C,o})}{RT_C} \tag{13}$$

where p_0 is the initial pressure (Pa), and $V_{H,0}$ and $V_{C,0}$ are the initial hot and cold volumes, respectively.

In this framework, the hot and cold volumes are defined as functions of the piston and displacer positions. The heater, cooler, and regenerator volumes are assumed to be zero, such that the dead volume arises solely from the engine kinematics and the relative motion of the piston and displacer, without contributions from the heat exchangers. With these assumptions, the effects of piston and displacer motion on engine performance can be evaluated without the influence of other non-ideal processes.

The present analysis is based on the classical Schmidt model, in which the working gas is assumed to behave as an ideal gas undergoing perfectly isothermal expansion and compression with perfect regeneration. Under these assumptions, the external heat supplied during one cycle is equal to the expansion work,

$$Q_H = \mathrm{W_e} = \oint p \, dV_H, \tag{14}$$

while the heat rejected during the isothermal compression equals the compression work,

$$Q_C = \mathrm{W_c} = \oint p \, dV_c. \tag{15}$$

and the corresponding thermal efficiency is calculated as

$$\eta = \frac{W_{\mathrm{net}}}{Q_H} = 1 - \frac{W_c}{W_e} \tag{16}$$

where W_{net} is the net cycle work (J), Q_H is the heat absorbed during the isothermal expansion (J), Q_C is the heat rejected during the isothermal compression (J), W_e is the expansion work (J), W_C is the compression work (J), and η_{th} is the thermal efficiency.

Since perfect regeneration is assumed, no additional external heat is required to compensate for the regenerative heat exchange, and the thermal efficiency is completely determined by the ratio of compression work to expansion work. In other words, efficiency is governed by the work ratio, so a cycle that more closely approaches the ideal Stirling process reduces compression losses relative to expansion work, increases the net work fraction, and therefore improves thermal efficiency.

III. Results and Discussions

A. Cycle deviation due to single sinusoidal piston and displacer trajectories

Figure 3(a) illustrates the ideal piston-displacer motion required to reproduce the ideal Stirling cycle. During 0° to 90°, the piston remains stationary while the displacer transfers the working gas from the cold space to the hot space. The decrease in cold volume is exactly balanced by the increase in hot volume, maintaining a constant total volume and producing the vertical constant-volume heating process in the P–V diagram (Figure 4). During 90° to 180°, the displacer remains fixed while the piston expands the hot volume, generating the ideal isothermal expansion. The reverse gas transfer occurs during 180° to 270°, where the piston remains stationary and the displacer redistributes the gas back to the cold space at constant

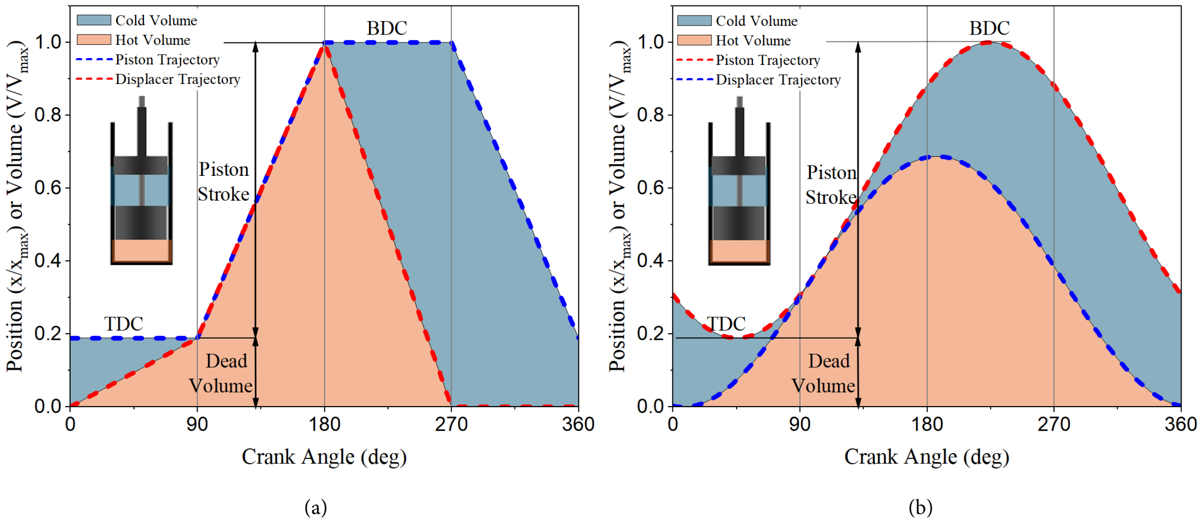

Figure 3. Piston and displacer trajectories and the corresponding working-fluid distribution for: (a) the ideal Stirling cycle; and (b) conventional sinusoidal motion.

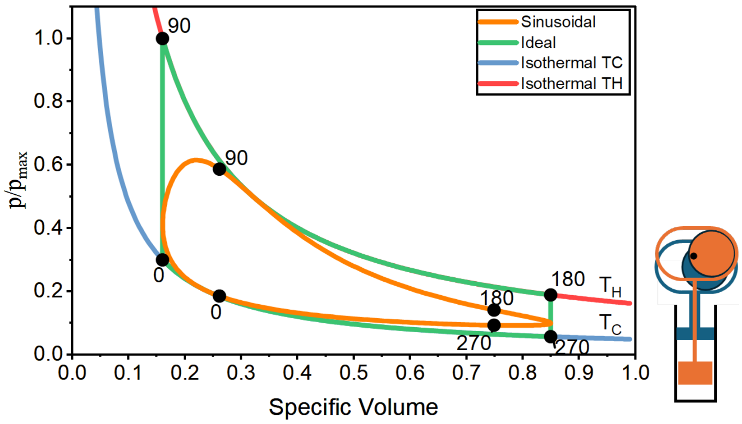

Figure 4. The rounded p-V diagram shows how the sinusoidal motion of the piston and displacer causes the Stirling cycle to deviate from its ideal form.

total volume, followed by isothermal compression during 270° to 360° as the piston compresses the gas while the displacer remains fixed. These four distinct motions produce the ideal Stirling cycle.

In contrast, Figure 3(b) shows the conventional sinusoidal crank mechanism used in practical beta-type Stirling engines. Unlike the ideal trajectory, both the piston and displacer move continuously throughout the crank rotation, causing the hot and cold volumes to change simultaneously. This continuously coupled motion prevents the engine from reproducing the two constant-volume processes of the ideal Schmidt cycle.

The deviation becomes particularly evident during the third quarter of the cycle (180° to 270°). Instead of maintaining a constant total volume as in Figure 3(a), both the piston and the displacer continue moving simultaneously in Figure 3(b). Although the displacer transfers gas from the hot space to the cold space, the piston also changes the total cylinder volume. Consequently, the increase in cold volume is no longer exactly balanced by the decrease in hot volume, causing the total working-gas volume to decrease continuously. This behavior is reflected in the orange P–V trajectory, where the process follows a sloped path rather than the vertical constant-volume cooling line of the ideal Stirling cycle.

A similar deviation occurs during the compression process (270° to 360°). In the ideal cycle, the displacer remains fixed while only the piston compresses the gas, ensuring that most of the working gas stays within the cold space throughout compression. However, under sinusoidal motion the displacer continues moving while the piston compresses the gas. As illustrated in Figure 3(b), part of the gas is simultaneously redistributed toward the hot space during compression, increasing the average gas temperature relative to the ideal case. Since the instantaneous pressure depends on both the total volume and the effective gas temperature, this non-ideal redistribution causes the pressure trajectory to remain above the ideal isothermal compression curve, as observed in the P–V diagram.

These differences can also be interpreted from the phase relationship between piston and displacer motion. In the ideal trajectory (Figure 3(a)), one component remains stationary while the other moves during each thermodynamic process, allowing independent control of gas transfer and volume variation. In contrast, the sinusoidal mechanism (Figure 3(b)) imposes continuous harmonic motion on both components, preventing complete decoupling between gas redistribution and volume change. As a result, compression or expansion occur simultaneously instead of sequentially, leading to deviation from the ideal Schmidt assumptions.

The cumulative effect of these deviations is evident in the P–V diagram (Figure 4). The sinusoidal cycle (orange curve) no longer contains the vertical constant-volume and exhibits a distorted expansion and compression path. Consequently, the enclosed cycle area is smaller than that of the ideal Stirling cycle (green curve), indicating a reduction in net indicated work. This reduction originates primarily from the inability of the sinusoidal mechanism to maintain the ideal distribution of working-gas volume between the hot and cold spaces during the gas-transfer processes. Therefore, optimizing the displacer trajectory to more closely approximate the ideal motion offers a direct means of increasing the enclosed P–V area and improving the thermodynamic performance of the beta-type Stirling engine. Overall, the sinusoidal motions of the piston and displacer introduce significant deviations from the ideal thermodynamic cycle, thereby reducing the net work output, as reported in previous studies [18].

B. The displacer motion trajectory derived from fourier-based optimization

The optimized cycle and trajectory, based on the Fourier series (equation (4)), are shown in Figure 5. The Fourier-based trajectory yields a continuous profile with smooth transitions in motion. These smooth transitions reduce inertial effects, thereby minimizing the force required to control the displacer motion.

In the 0° to 90° interval, corresponding to the end of compression and the beginning of expansion. During the final stage of compression (0° to 45°), the first-order case yields the smallest hot-side volume and the lowest pressure. The small hot-side volume provides the closest approximation to isothermal compression at T_C (shown by the blue line in Figure 5). Higher Fourier orders further reduce the hot volume. However, it remains slightly larger than in the first-order case. The process approach is isothermal compression behavior. In the early expansion stage (45° to 90°), increasing the Fourier order reduces the cold-side volume. At the same time, it increases the expansion pressure. As a result, the process better approximates isothermal expansion (shown by the red line in Figure 5).

In the 90° to 180° interval, the addition of higher Fourier orders enhances the expansion process. Specifically, it increases the displacer stroke and prolongs the duration during which the displacer follows the piston motion. As a result, the cold-side volume is minimized for a longer period, extending the portion of isothermal expansion at T_H.

For the 180° to 270° interval, higher Fourier orders improve both the end of expansion (180° to 225°) and the beginning of compression (225° to 270°). At the end

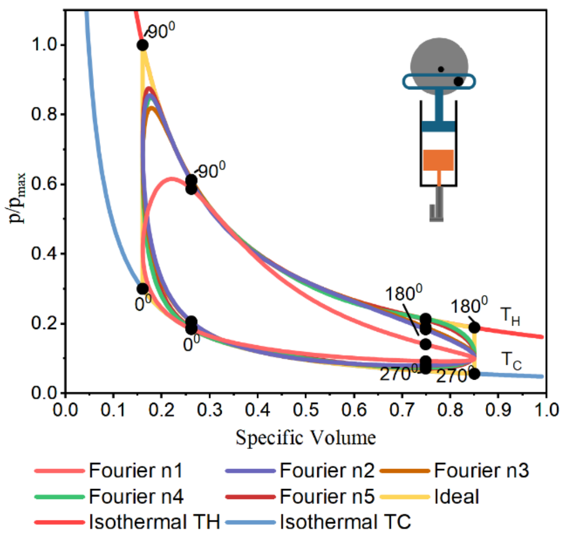

(a)

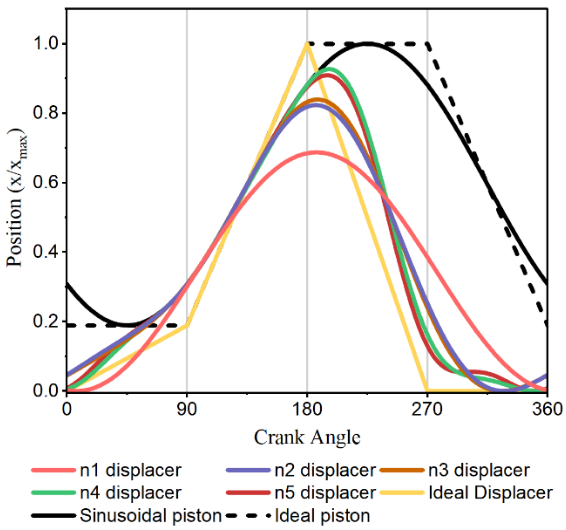

(b)

Figure 5. Influence of Fourier order on: (a) working-area enlargement; and (b) displacer trajectories.

of expansion, increasing the Fourier order enlarges the displacer stroke and increases the hot-side volume, thereby approaching isothermal expansion more closely at T_H. At the onset of compression, higher-order harmonics increase the slope of the trajectory, reducing the hot-side volume and further improving the approach toward isothermal behavior.

In the 270° to 360° interval, the addition of higher harmonics continues to improve the cycle by reducing the hot-side volume fraction, lowering the working fluid temperature, and bringing the process closer to isothermal compression. Overall, increasing the Fourier order significantly enhances cycle performance. The ideal work ratio increases significantly by 20 % from the first to the fourth order, as shown in Table 2. However, further increases beyond the fourth order do not result in substantial improvements in the cycle. Subsequently, the optimization is performed using a fourth-order model.

As shown in Figure 6(a), the piston and displacer trajectories for different stroke lengths share similar characteristics, differing only in amplitude scaling. The phase relationship between the piston and displacer remains unchanged, indicating that the fundamental shape of the trajectory is preserved. In the P–V diagram (see Figure 6(b)), the cycle area remains identical across

Table 2.
Percentage of ideal work for different fourier orders.

Fourier Order	Fraction of Ideal Work (%)
1	69.8
2	86.2
3	86.9
4	91.9
5	92.1
6	92.4

all stroke variations, showing that changes in stroke length affect only the volume scale without altering the underlying thermodynamic cycle. Both expansion and compression processes continue to follow behavior close to the ideal Stirling cycle.

Furthermore, the ratio of displacer to piston position (see Figure 6(c)) exhibits the same trend across all stroke variations, indicating that the proportion of working fluid between the hot and cold spaces remains constant. This consistency explains why system performance remains unchanged despite variations in stroke length. Physically, this shows that stroke variation does not affect efficiency or work output if the CR is maintained, confirming that the optimal

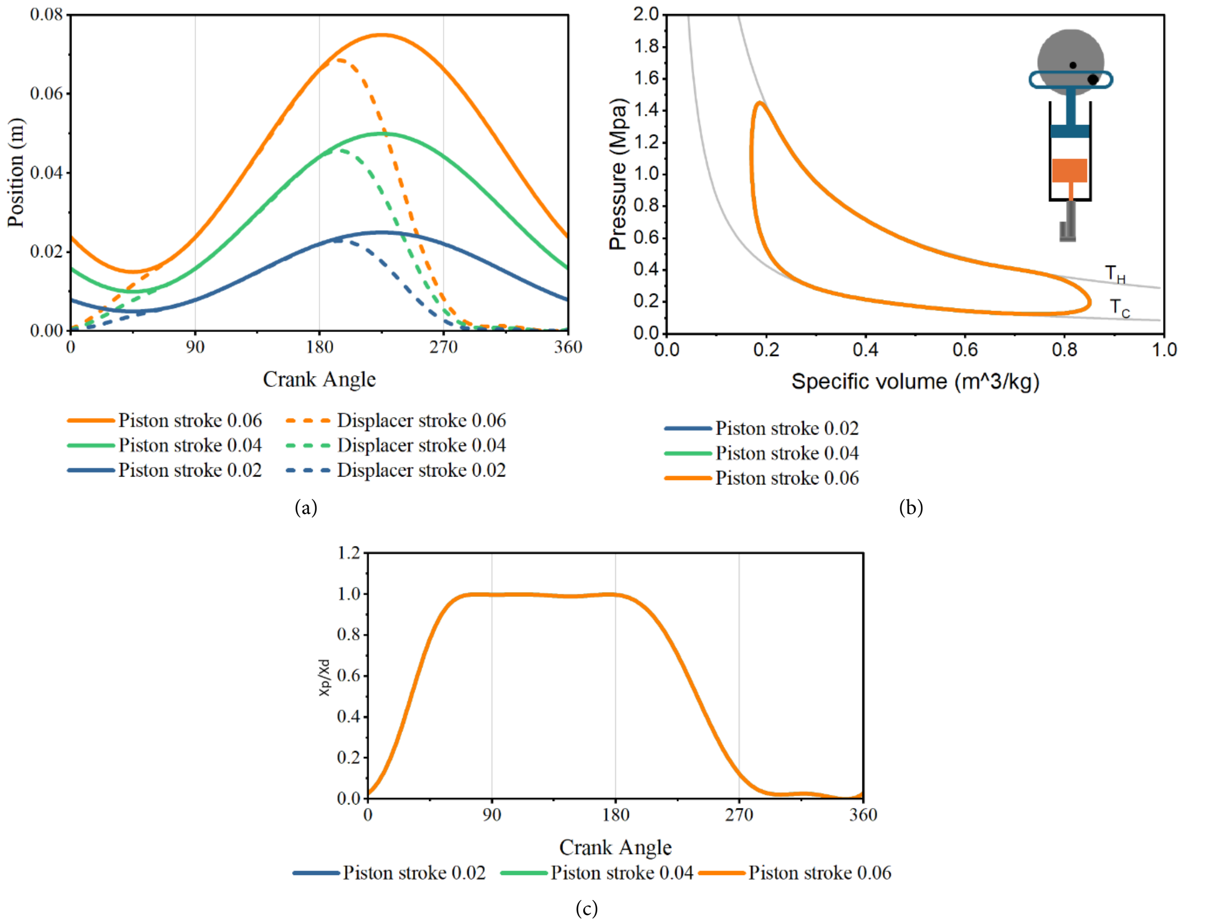

Figure 6. Effect of stroke length on: (a) trajectory characteristics; (b) p-V diagram; and (c) displacer position relative to piston position.

trajectory is scale-invariant with respect to stroke length.

Based on Figure 6, variations in CR (CR 2 to 5) significantly affect the trajectory characteristics: the piston and displacer curves no longer exhibit the simple scaling behavior observed in stroke variation but instead undergo notable shape changes (see Figure 7(a)). As the CR increases, the amplitude and motion profile of the displacer adjust to accommodate the altered volume distribution between the hot and cold spaces, thereby shifting the phase relationship between the piston and the displacer. This indicates that the Fourier-based trajectory is strongly dependent on the CR.

The p–V diagram (see Figure 7(b)) shows that increasing the CR substantially enlarges the cycle area, which directly corresponds to higher net work output. Higher CR values produce greater maximum pressures and smaller minimum volumes, yielding a wider cycle. This trend is confirmed by the tabulated data (Table 3), in which the specific work increases from 123 kJ/kg to 299 kJ/kg.

Furthermore, the ratio of displacer to piston position (x_D/x_P) exhibits distinct profiles for each CR

Table 3.
Percentage of ideal work for different CRs.

CR	Fraction of Ideal Work (%)	Specific Work (kJ/kg)
2	88	123
3	91	200
4	91	253
5	92	299

(see Figure 7(c)). Differences are particularly evident during the transition from expansion to compression, indicating a shift in the timing of fluid transfer. This variation suggests that the proportion of dynamic volume distribution between the hot and cold spaces is no longer constant as the CR changes.

Physically, these results confirm that the CR has a fundamental influence on both the thermodynamic and kinematic behavior of the system. Unlike stroke variation, changes in CR alter the cycle's boundary conditions, preventing the optimal trajectory from being preserved in the same form. Therefore, the trajectory cannot be scaled directly across different compression ratios and must be re-optimized for each CR.

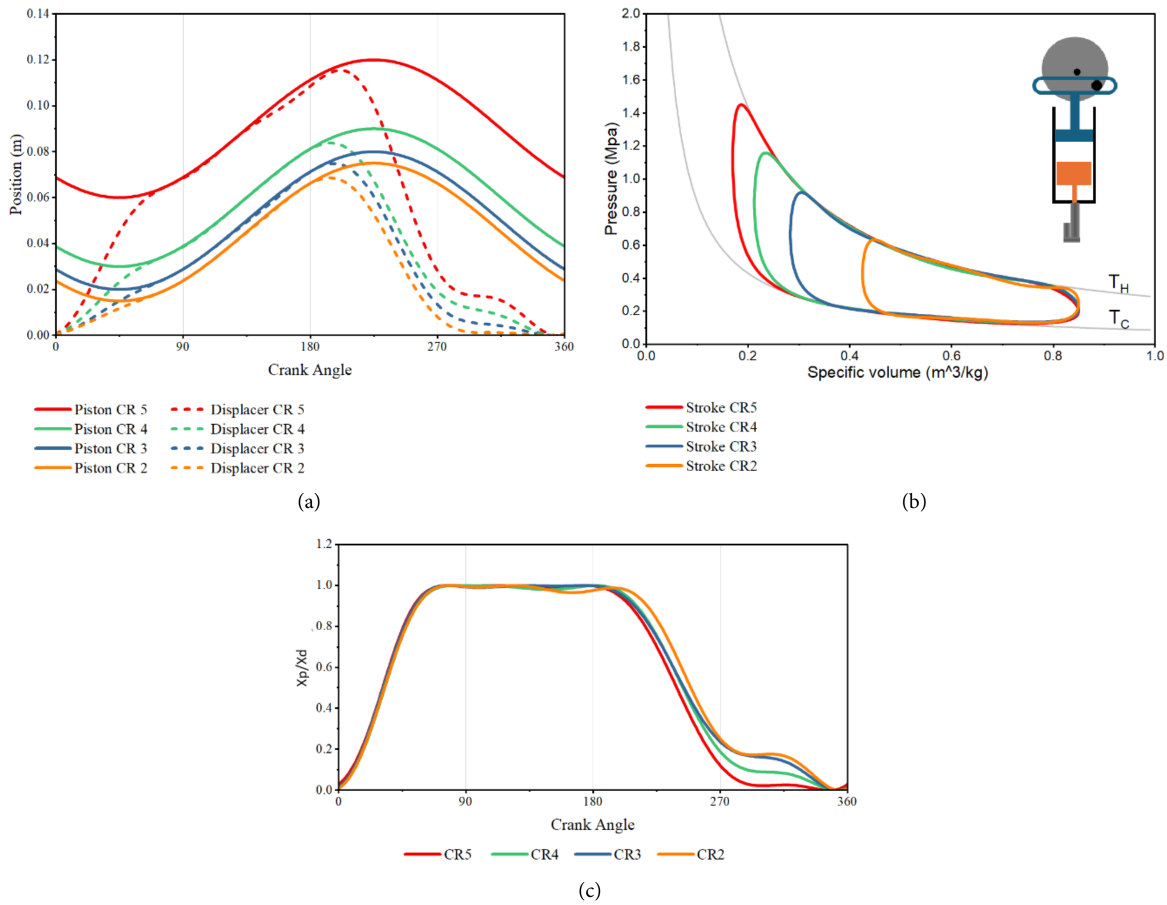

Figure 7. Effect of CR on; (a) trajectory characteristics; (b) p-V diagram; and (c) displacer position relative to piston position.

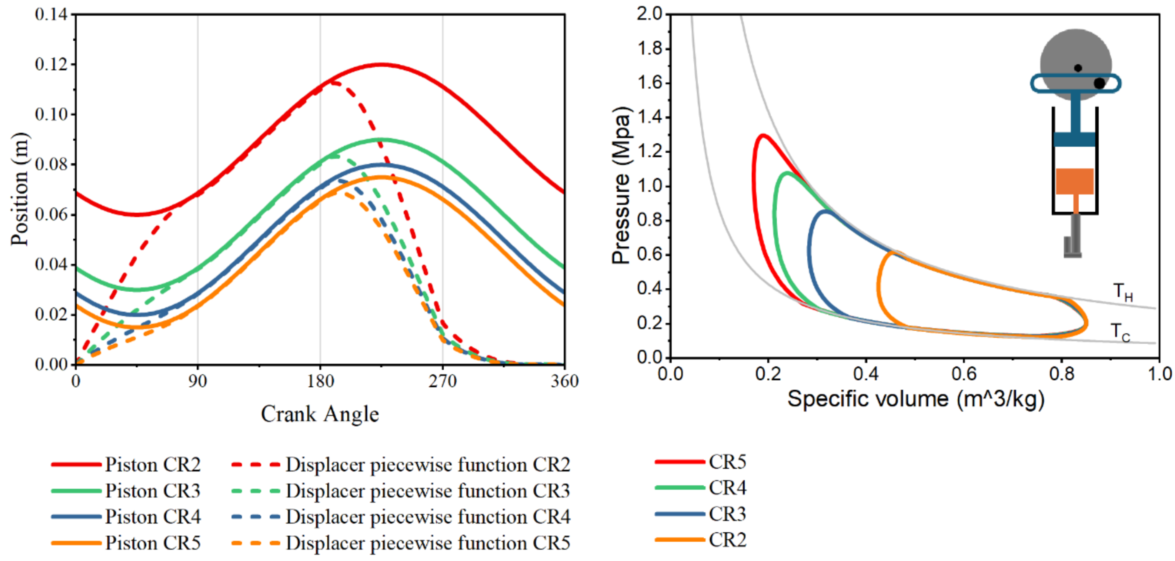

(a) (b)

Figure 8. (a) Trajectory and (b) p-V diagram of the piecewise function CR 1-5.

C. General equation of the Fourier base optimum trajectory

To obtain a generalized formulation (Equation (5)) applicable across a range of CRs, the shape function is averaged from optimized Fourier-based trajectories corresponding to CRs 2, 3, 4, and 5. The shape constant is subsequently fine-tuned to prevent collision between the piston and the displacer. The shape function is shown in Table 4.

Table 4.
Shape constants for each segment.

Crank Angle	Shape Constant			
	σ0	σ1	σ2	σ3
$0 \le \theta \le 90$	0	0.5	0.9	0.99
$90 \le \theta \le 180$	0.99	0.99	0.99	0.99
$180 \le \theta \le 270$	0.99	0.87	0.55	0.15
$270 \le \theta \le 360$	0.15	0.04	0.01	0

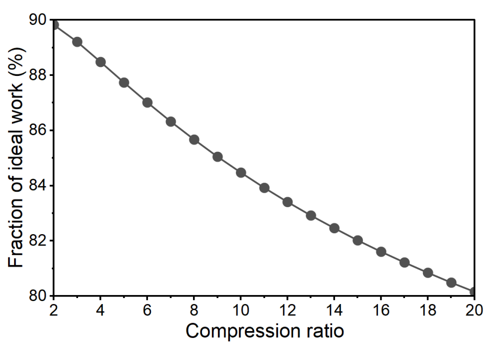

Figure 9. The performance of the piecewise trajectory across various CRs demonstrates its robustness, achieving over 80 % of the ideal work even at CRs as high as 20.

Figure 8(a) shows the displacer trajectory and Figure 8(b) the pV diagram. The use of an averaged shape function derived from CRs in the range of 2 to 5 reduces the work ratio by approximately 2 % from the 4th Fourier base trajectory. Nevertheless, the piecewise function approach remains applicable across a broader range of CRs, including high ones, as shown in Figure 9. When CR = 20, the piecewise function performs relatively well, achieving approximately 80 % of the ideal work.

D. Comparison with traditional mechanisms result

A comparative evaluation is conducted to assess the performance of control mechanisms (Fourier-based and piecewise-based) against conventional mechanisms (crank, Scotch yoke, and rhombic drive). To ensure a fair comparison, the stroke length and sweep volume are kept the same across all mechanisms [10][11]. The engine parameters used in the analysis are listed in Table 5.

In the crank angle range of 0° to 90°, the process consists of two stages: compression (0° to 45°) followed by expansion (45° to 90°), as shown in Figure 9. During this interval, the displacer moves toward the piston, transferring the working fluid from the cold space to the hot space. In conventional mechanisms, the proportion of cold space during compression is greater than in controlled approaches such as Fourier-based or piecewise-trajectory approaches. This condition results in lower compression pressure as shown in Figure 10(a). However, it also leads to a smaller available hot space during expansion. Overall, within the 0° to 90° interval, controlled mechanisms produce higher work output.

This indicates that maximizing the expansion process has a greater impact on increasing net work than minimizing compression work as stated in [11].

In the crank angle range of 90° to 180°, the process is characterized by expansion. The displacer follows the piston's motion. The synchronized motion helps maximize the volume of hot space throughout the expansion process. Controlled mechanisms achieve a higher hot-volume proportion during this phase than conventional mechanisms. As a result, the expansion process approaches isothermal conditions more closely, thereby improving thermodynamic cycle performance.

In the crank angle range of 180° to 270°, the process consists of two stages: expansion (180° to 225°) followed by compression (225° to 270°). In both stages, controlled mechanisms produce higher net work than conventional mechanisms. This improvement is achieved through enhanced expansion work and reduced compression work. During expansion, the controlled approach utilizes a longer displacer stroke, allowing the displacer to follow the piston motion for a longer duration. This results in a larger hot space volume and enables a more effective expansion process. During compression, the controlled mechanism generates a greater proportion of cold space, thereby reducing the required compression work. The combined effect results in greater net work.

In the crank angle range of 270° to 360°, the displacer continues to move toward the cylinder wall. In controlled mechanisms, the displacer reaches the wall earlier than in conventional mechanisms. As a result, the fraction of fluid in the hot volume is reduced, and most of the working fluid is concentrated in the cold volume. This condition leads to lower pressure during compression. In addition, the compression process more closely approaches isothermal behavior at lower temperatures, thereby reducing the required compression work.

Table 5.
Geometric parameters and operating conditions used for the performance comparison of the investigated Stirling engine mechanisms.

Parameter	Rhombic	Crank	Scotch Yoke	Fourier	Piecewise
Piston stroke (m)	0.06	0.06	0.06	0.06	0.06
Crank radius (m)	0.03	0.03	0.03	0.03	0.03
Piston diameter (m)	0.04	0.04	0.04	0.04	0.04
Piston area (m^2)	0.0028	0.0028	0.0028	0.0028	0.0028
Hot temperatur (K)	1000	1000	1000	1000	1000
Cold temperatur (K)	300	300	300	300	300
Fluid	Air	Air	Air	Air	Air
Charge pressure (Pa)	101325	101326	101327	101328	101329
Displacer connecting rod length(m)	0.33	0.3	-	-	-
Piston connecting rod length(m)	0.3	0.3	-	-	-
Center gear distance (m)	0.24	-	-	-	-
Length of rhombic linkage (m)	0.07	-	-	-	-

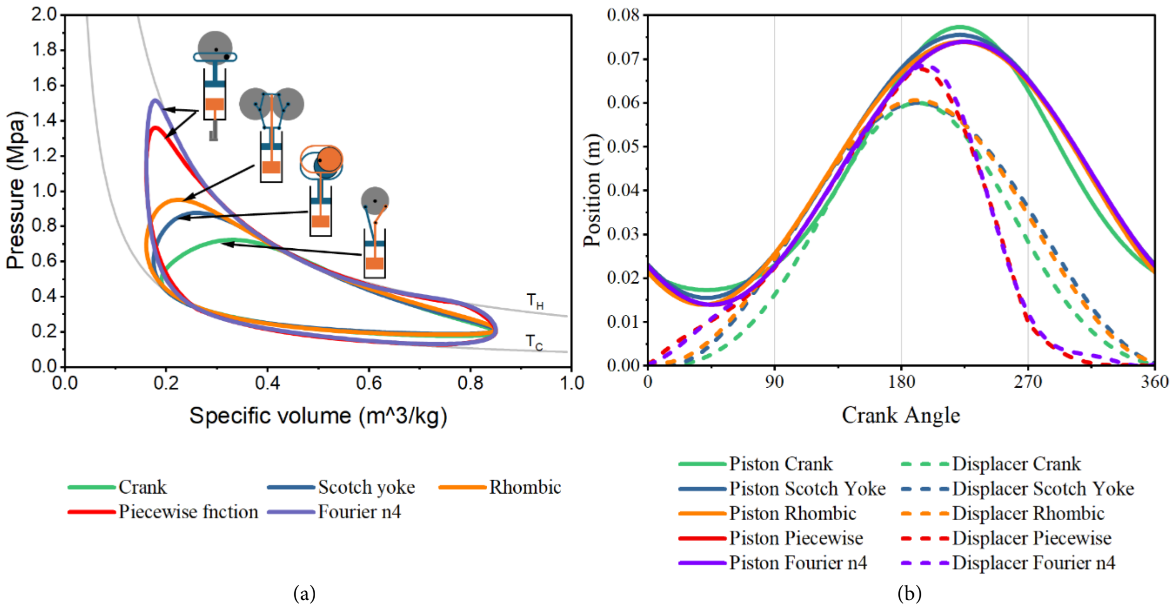

Figure 10. A comparison of the results of the piecewise function for: (a) cycle; and (b) trajectory to those of other mechanisms.

Table 6.
Percentage of ideal work for different mechanisms.

Mechanism	Fraction of Ideal Work (%)	Work (J)	Eficiency (%)
Crank	59.8	46.3	53.3
Scotch yoke	66.0	52.7	55.5
Rhombic	68.5	56.5	56.7
Piecewise function	88.8	72.1	64.9
Fourier n4	91.9	74.8	65.8

There is a slight difference in the cycle characteristics between the Fourier-based control mechanism and the piecewise-function approach. During the early expansion phase (45° to 90°), the pressure in the piecewise-based mechanism tends to be lower than that of the Fourier-based approach. This difference is influenced by the adopted shape function, from which the Fourier-based formulation is derived based on the averaged ratio of displacer to piston positions over a CR range of 2 to 5. As a result, in the piecewise approach, the distance between the displacer and the piston increases, leading to a larger cold-space fraction and a lower working-gas pressure during the initial expansion period. Nevertheless, this difference has only a minor influence on the overall cycle performance, as the fraction of ideal work differs by only about 2 %, corresponding to net works of 72.1 J and 74.8 J, respectively (Table 6).

A similar trend is observed in the thermal efficiency. The conventional mechanisms exhibit efficiencies ranging from 53.3 % for the crank mechanism to 56.7 % for the rhombic drive, whereas the proposed piecewise-function and Fourier-based mechanisms achieve thermal efficiencies of 64.9 % and 65.8 %, respectively. These values represent an improvement of approximately 8 to 12 percentage points over the conventional mechanisms. Under the Schmidt-model assumptions of ideal isothermal processes and perfect regeneration, the heat input is equal to the expansion work; therefore, an increase in the ratio of net work to expansion work directly translates into higher thermal efficiency. Consequently, the proposed displacer trajectories not only increase the fraction of ideal work but also improve the thermodynamic efficiency of the cycle. Although the Fourier-based mechanism provides the highest work output and thermal efficiency, the piecewise-function approach achieves nearly identical performance while offering a considerably simpler mathematical formulation and facilitating practical implementation.

IV. Conclusion

This study shows that optimizing the displacer trajectory using a Fourier-based approach and then simplifying it to a piecewise function significantly improves the thermodynamic performance of a beta-type Stirling engine. The proposed method approximates the ideal Stirling cycle by controlling displacer motion, yielding expansion and compression processes that more closely approach isothermal conditions. The optimized trajectory achieves approximately 92 % of the ideal work output, outperforming conventional sinusoidal mechanisms. Furthermore, the piecewise representation preserves the key characteristics of the optimized trajectory while enabling robust applicability across a wide range of geometries and compression ratios without requiring re-optimization. These findings confirm that trajectory design is a critical factor in improving cycle efficiency and highlight the proposed approach as a practical and effective solution for advanced Stirling engine development. For future work, this study will be extended to experimental implementation by developing and testing a physical prototype. A prototype incorporating displacer-motion correction based on a Scotch yoke mechanism with variable connecting-rod length will be investigated. This approach is expected to enable the practical realization of the proposed trajectory control and further evaluate its effectiveness under real operating conditions.

Acknowledgements

R. Hakim would like to acknowledge Universitas Jenderal Achmad Yani for providing financial support throughout the doctoral study.

Declarations

Author contribution

R. Hakim: Writing - Original Draft, Writing - Review & Editing, Conceptualization, Methodology, Formal analysis, Investigation, Data Curation, Visualization. **T. Hardianto**: Writing - Review & Editing, Supervision, Methodology, Visualization. **P. Sutikno**: Writing - Review & Editing, Supervision, Methodology, Visualization. **P. Sambegoro**: Writing - Review & Editing, Supervision, Methodology, Visualization.

Funding statement

This research was funded by the supervisor's personal program and personal funds.

Competing interest

The authors declare that they have no known competing financial interests or personal relationships that could have appeared to influence the work reported in this paper.

The use of AI or AI-assisted technologies

The authors used OpenAI/ChatGPT and Grammarly to check for grammatical errors and increase language clarity while preparing this work. The authors took full responsibility for the publication's content after using this tool/service and reviewed and edited it as necessary.

Additional information

Reprints and permission: information is available at https://mev.brin.go.id/.

Publisher's Note: National Research and Innovation Agency (BRIN) remains neutral with regard to jurisdictional claims in published maps and institutional affiliations.

References

[1] D. Roy *et al.*, "Techno-economic and environmental analyses of a solar-assisted Stirling engine cogeneration system for different dwelling types in the United Kingdom," *Energy Convers. Manag.*, vol. 302, Feb. 2024.

[2] K. Laazaar and N. Boutammachte, "New approach of decision support method for Stirling engine type choice towards a better exploitation of renewable energies," *Energy Convers. Manag.*, vol. 223, Nov. 2020.

[3] A. C. Ferreira, J. Silva, S. Teixeira, J. C. Teixeira, and S. A. Nebra, "Assessment of the Stirling engine performance comparing two renewable energy sources: Solar energy and biomass," *Renewable Energy*, vol. 154, pp. 581–597, 2020.

[4] R. Pido, S. Humena, and F. Abdullah, "Performance study of corncob-fueled updraft gasification with integrated solar power plant as a supporting energy source for the reactor," *Journal of Mechatronics, Electrical Power, and Vehicular Technology*, vol. 16, no. 2, Dec. 2025.

[5] S. S. Jaafar, H. A. Maarof, H. B. Hamasalh, and K. M. Ahmed, "Comparative performance evaluation of dual-axis solar trackers: Enhancing solar harvesting efficiency," *Journal of Mechatronics, Electrical Power, and Vehicular Technology*, vol. 15, no. 1, pp. 23–31, 2024.

[6] K. Wang, S. R. Sanders, S. Dubey, F. H. Choo, and F. Duan, "Stirling cycle engines for recovering low and moderate temperature heat: A review," *Renewable and Sustainable Energy Reviews*, vol. 62, pp. 89–108, 2016.

[7] S. Zare, A. R. Tavakolpour-saleh, A. Aghahosseini, M. H. Sangdani, and R. Mirshekari, "Design and optimization of Stirling engines using soft computing methods: A review," *Appl. Energy*, vol. 283, Feb. 2021.

[8] F. Xin, B. Xu, D. Dai, W. Liu, and Z. Liu, "Evaluation of heat transfer enhancement effect at the hot/cold end of a Stirling engine using performance improvement factor," *Energy*, vol. 311, Dec. 2024.

[9] F. Aksoy *et al.*, "Effects of the regenerator on engine performance of a rhombic drive beta type stirling engine," *Energy Sources, Part A: Recovery, Utilization and Environmental Effects*, vol. 47, no. 1, pp. 6665–6673, 2025.

[10] D. Erol, "An experimental comparative study of the effects on the engine performance of using three different motion mechanisms in a beta-configuration Stirling engine," *Energy*, vol. 293, p. 130660, 2024.

[11] H.-S. Yang, H.-Q. Zhu, and X.-Z. Xiao, "Comparison of the dynamic characteristics and performance of beta-type Stirling engines operating with different driving mechanisms," *Energy*, vol. 275, p. 127535, 2023.

[12] A. Hadidi, "Enhanced design of Stirling engines via multi-objective optimization: Effects of dead volumes, regenerator effectiveness, and operating parameters," *Case Studies in Thermal Engineering*, vol. 77, p. 107582, Jan. 2026.

[13] T. Ergin, "Experimental optimization of displacer working gap in a gamma-type Stirling engine," *Engineering Science and Technology, an International Journal*, vol. 52, Apr. 2024.

[14] D. Erol, H. Yaman, and B. Doğan, "A review development of rhombic drive mechanism used in the Stirling engines," *Elsevier Ltd.*, vol. 78, 2017, p. 1044-1067.

[15] J. Podešva and Z. Poruba, "The Stirling engine mechanism optimization," *Perspect. Sci. (Neth).*, vol. 7, pp. 341–346, Mar. 2016.

[16] H. Bi, J. Yang, C. Chen, and B. Luo, "Heat transfer and flow characteristics of intermittent oscillating flow in tube," *Appl. Therm. Eng.*, vol. 225, May 2023.

[17] M. Nicol-Set and D. Nobes, "Experimental evaluation of piston motion modification to improve the thermodynamic power output of a low temperature gamma Stirling engine," *in E3S Web of Conferences, EDP Sciences*, Oct. 2021.

[18] S. Ranieri, G. A. O. Prado, and B. D. MacDonald, "Efficiency reduction in stirling engines resulting from sinusoidal motion," *Energies (Basel).*, vol. 11, no. 11, Nov. 2018.

[19] M. Farid Zainudin, R. Abu Bakar, K. Al Kadirgama, and G. Leong Ming, "Kinematic and thermodynamic operational analysis of rhombic-drive Stirling engine

prototype," *in IOP Conference Series: Materials Science and Engineering*, vol. 788, Jun. 2020.

[20] M. Craun and B. Bamieh, "Optimal periodic control of an ideal stirling engine model," *Journal of Dynamic Systems, Measurement and Control, Transactions of the ASME*, vol. 137, no. 7, Jul. 2015.

[21] H. Tian, S. Zhao, S. Kuang, and Y. Gong, "Enhanced thermodynamic performance of a modified α type Stirling engine with fine-tuned piston trajectories controlled via staircase decomposed target signals," *Case Studies in Thermal Engineering*, vol. 73, p. 106512, Sep. 2025.

[22] E. Öztürk, "Optimization of a novel drive mechanism approaching the ideal cycle for beta type Stirling engines," *Engineering Science and Technology, an International Journal*, vol. 47, p. 101555, Nov. 2023.

[23] H. M. Wong and S. Y. Goh, "Experimental comparison of sinusoidal motion and non-sinusoidal motion of rise-dwell-fall-dwell in a Stirling engine," *Journal of Mechanical Engineering and Sciences*, vol. 14, no. 3, pp. 6971–6981, Sep. 2020.

[24] H. M. Wong, R. Bahar, and Y. S. Ong, "Experimental evaluation of the displacer and working piston hybrid motion to improve the performance of a stirling engine," *Appl. Therm. Eng.*, vol. 279, Nov. 2025.

[25] W. Ye, T. Zhang, X. Wang, Y. Liu, and P. Chen, "Parametric study of gamma-type free piston stirling engine using nonlinear thermodynamic-dynamic coupled model," *Energy*, vol. 211, Nov. 2020.

[26] R. Sharma and B. Glemmestad, "On generalized reduced gradient method with multi-start and self-optimizing control structure for gas lift allocation optimization," *J. Process Control*, vol. 23, no. 8, pp. 1129–1140, 2013.

[27] H. Hachem, R. Gheith, F. Aloui, and S. Ben Nasrallah, "Technological challenges and optimization efforts of the Stirling machine: A review," *Energy Conversion and Management*., vol. 171, pp. 1365-1387, 2018.

[28] S. A. Salih, B. A. Aljashaami, N. T. Alwan, M. A. Qasim, S. E. Shcheklein, and V. I. Velkin, "Isothermal thermodynamic analysis investigation of the Stirling engine types (alpha, beta, gamma): A theatrical study," *Mater. Today Proc.*, 2023.